Effect of Chain Length on the Photophysical Properties of Pyrene-Based Molecules Substituted with Extended Chains

4 AUTHORS, INCLUDING:

Digambara Patra
American University of Beirut
68 PUBLICATIONS   **1,497** CITATIONS

SEE PROFILE

Bilal R Kaafarani
American University of Beirut
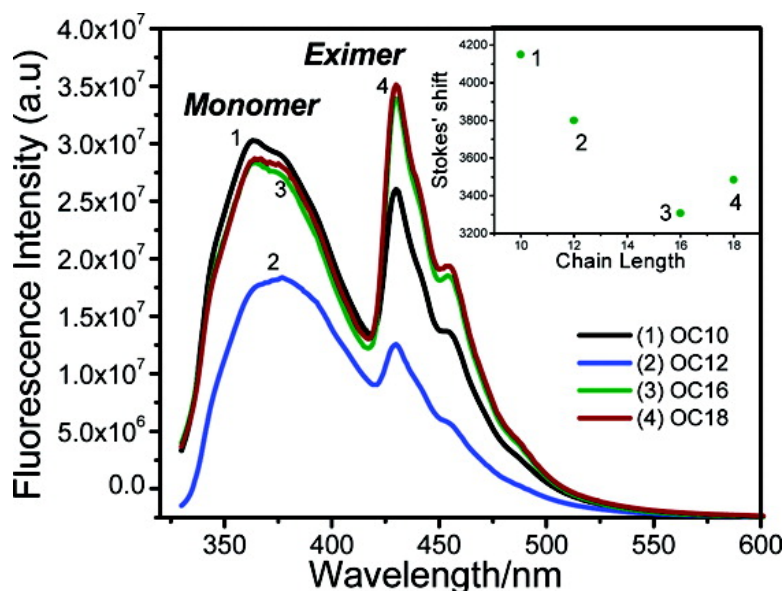**55** PUBLICATIONS   **969** CITATIONS

SEE PROFILE

Article

Effect of Chain Length on the Photophysical Properties of Pyrene-Based Molecules Substituted with Extended Chains

Jad A. Degheili, Rasha M. Moustafa, Digambara Patra, and Bilal R. Kaafarani

More About This Article

Additional resources and features associated with this article are available within the HTML version:

- Supporting Information
- Access to high resolution figures
- Links to articles and content related to this article
- Copyright permission to reproduce figures and/or text from this article

View the Full Text HTML

Effect of Chain Length on the Photophysical Properties of Pyrene-Based Molecules Substituted with Extended Chains

Jad A. Degheili, Rasha M. Moustafa, Digambara Patra,* and Bilal R. Kaafarani*

Department of Chemistry, American University of Beirut, Beirut 1107-2020, Lebanon

Received: August 8, 2008

The important role played by organic conjugated compounds in the fields of electronics and optoelectronics has led to a vast field of research concerned with synthesizing various complex structures where $\pi-\pi$ stacking plays a vital role. Pyrene-based molecules are examples of compounds which allow efficient charge transfer through $\pi-\pi$ molecular stacking. Photophysical studies of such compounds have shown similar behavior as that of pyrene, even though they bear two additional conjugated rings and four long alkyl chains. Chain length may have played an effective role in influencing the $\pi-\pi$ molecular stacking of such molecules. In continuation of our earlier work (Moustafa, R. M.; Degheili, J. A.; Patra, D.; Kaafarani, B. R. *J. Phys. Chem. A* **2008**, *113*, 1235–1243), we hereby synthesize and investigate the role of the chain lengths on the photophysical aspects of 2,11-di-*tert*-butyl-6,7,15,16-tetrakis(alkoxy/alkythio)quinoxaline-[2′,3′:9,10]phenanthro[4,5-*abc*]phenazine, TQPP-[*t*-Bu]$_2$-[XR]$_4$ (X = O, S; R = C$_n$H$_{2n+1}$). Various photophysical parameters such as Stokes shift, fluorescence lifetime, fluorescence quantum yield, and radiative and nonradiative rate constants are evaluated for TQPP-[*t*-Bu]$_2$-[OR]$_4$ and TQPP-[*t*-Bu]$_2$-[SR]$_4$ in tetrahydrofuran. The variation of the Stokes shift, fluorescence quantum yield, and lifetime are also correlated with the number of carbons in the alkyl chain R for TQPP-[*t*-Bu]$_2$-[OR]$_4$ and TQPP-[*t*-Bu]$_2$-[SR]$_4$.

1. Introduction

The field of organic semiconductors has undergone tremendous progress in the last 15 years due to their exciting electronic and optoelectronic properties, which have enabled development of improved electronic devices.[2] Organic semiconductors include conjugated polymers, conjugated oligomers, and small conjugated molecules that can self-assemble and exhibit interesting electronic and optoelectronic properties.[3] Some of these find applications in organic field-effect transistors (OFETs),[4] organic light-emitting diodes (OLEDs),[5] organic photovoltaic cells (OPVs),[6] and sensors.[3] New organic semiconductors, such as thiophene oligomers and acenes (e.g., pentacenes),[4,7,8] have been extensively studied in order to achieve better carrier mobility, sensitivity, and stability in the device. For example, a *p*-channel thin-film field-effect transistor of solution-processed pentacene showed a hole mobility as high as 0.89 cm^2 V^{-1} s^{-1}.[2] Despite this work, the best mobilities achieved for organic semiconductors are still less than that of polycrystalline silicon;[9] however, organic semiconductors have the advantages of structural flexibility and the potential for good solubility which allows for low-cost solution processing at low temperatures, with the possibility of fabricating large-area devices.[3] Their disadvantages include difficulties in achieving high levels of purity, lower mobilities than inorganic semiconductors, and poor thermal and mechanical stability.[3] The low mobility of organic semiconductors is limited by their weak van der Waals interactions, in contrast to the strong covalent and ionic forces found in inorganic systems.[2]

A very interesting class of organic semiconductors is that of discotic liquid crystals (DLCs); these materials have exciting elect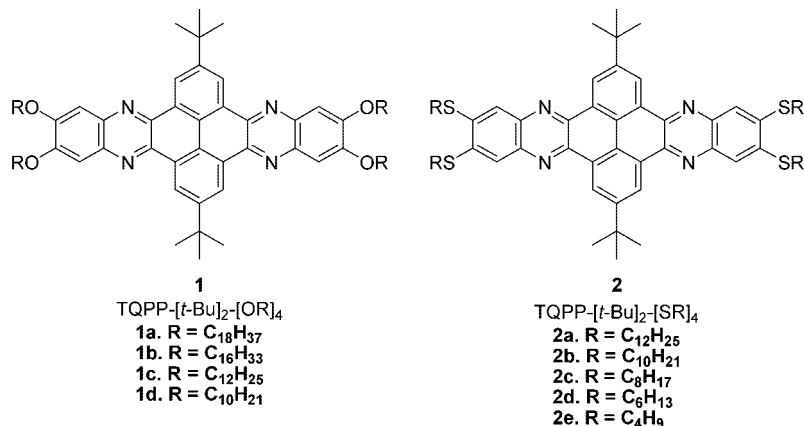ronic and optoelectronic properties and can readily be processed into films,[10] making them ideal building blocks for smart materials in organic-based electronic and optoelectronic devices such as OLEDs,[11] OPVs,[12] and OFETs.[13] DLCs are usually formed of a rigid core to which 3 to 8 flexible chains are attached; these materials self-organize into columnar stacks within which effective $\pi-\pi$ orbital overlap leads to high intrastack charge-carrier mobilities that allow the transportation of the charges in a one-dimensional manner.[14] Mobility values as high as 0.5 cm^2 V^{-1} s^{-1} have been reported in some discotic mesophases, such as those formed by hexabenzocoronene derivatives.[15] However, many of the detailed photophysical and photochemical properties of compounds of this type remain to be investigated. The chain length in DLCs is well-known to affect their mesophase behavior.[10] In this paper, we report the effect of chain length on the photophysical behavior of two series of pyrene-based molecules: 2,11-di-*tert*-butyl-6,7,15,16-tetrakis(alkoxy/alkythio)quinoxaline[2′,3′:9,10]phenanthro[4,5-*abc*]phenazine, TQPP-[*t*-Bu]$_2$-[XR]$_4$ (X = O, S; R = C$_n$H$_{2n+1}$) (Figure 1). Detailed photophysical studies on four of these pyrene-based molecules (**1c**, **1d**, **2a**, and **2b**) have been reported elsewhere.[1] An investigation of the mesophase behavior in these materials is currently ongoing.

Chain length may play a role in determining the effectiveness of the $\pi-\pi$ molecular orbital stacking in such compounds and, thus, the mobility of charge carriers across nearby molecules. This paper reports further investigations that were made using a more extensive range of alkyl groups to understand how chain length affects the Stokes shift, fluorescence quantum yield, fluorescence lifetime, and radiative and nonradiative rate constants, as well as the absorption properties in tetrahydrofuran solvent.

2. Experimental Section

Chemicals and solvents were purchased from Acros. Standard grade silica gel (60 Å, 32−63 μm) and silica gel plates (250

* Corresponding authors. E-mail: dp03@aub.edu.lb (D.P.); bilal.kaafarani@aub.edu.lb (B.R.K.). Telephone: +961-1-350 000. Fax: +961-1-365217.

Photophysical Properties of Pyrene-Based Molecules

J. Phys. Chem. A, Vol. 113, No. 7, 2009 **1245**

Figure 1. Structures of TQPP-[*t*-Bu]$_2$-[XR]$_4$ (X = O, S; R = C$_n$H$_{2n+1}$).

μm) were purchased from Sorbent Technologies. Reactions that required anhydrous conditions were carried out under argon in oven-dried glassware. A Bruker spectrometer was used to record the NMR spectra. CDCl$_3$ was the solvent for NMR, and chemical shifts relative to tetramethylsilane (TMS) at 0.00 ppm are reported in parts per million (ppm) on the δ scale. The MALDI data were acquired at the Bioanalytical Mass Spectrometry Facility at the Georgia Institute of Technology, Atlanta, GA. Elemental analyses were performed at Atlantic Microlab Inc., Norcross, GA.

The general synthesis of TQPP-[*t*-Bu]$_2$-[OR]$_4$ and TQPP-[*t*-Bu]$_2$-[SR]$_4$ is described elsewhere.[1] After column chromatography using CHCl$_3$ as eluent, the compounds were recrystallized from nitrobenzene (for **1a** and **1b**) and toluene (for **2c**, **2d**, and **2e**). Spectroscopic data of TQPP-[*t*-Bu]$_2$-[XR]$_4$ (X = S, O; R = C$_{12}$H$_{25}$ and C$_{10}$H$_{21}$) are reported elsewhere.[1]

2,11-Bis(1-methylethyl)-6,7,15,16-tetrakis(octadecyloxy)quinoxaline[2′,3′:9,10]phenanthro[4,5-*abc*]phenazine, TQPP-[*t*-Bu]$_2$-[OC$_{18}$H$_{37}$]$_4$ (1a). Yellow solid **1a** (0.25 g, 25%), mp 173−175 °C. ^{1}H NMR (300 MHz, CDCl$_3$): δ 0.87 (12H, t, *J* = 6.7 Hz), 1.26 (112H, m), 1.58 (8H, m), 1.76 (18H, s), 2.03 (8H, quintet, *J* = 7.4 Hz), 4.33 (8H, t, *J* = 6.5 Hz), 7.64 (4H, s), 9.73 (4H, s). ^{13}C NMR (75.5 MHz, CDCl$_3$, 45 °C): δ 14.07, 22.70, 26.16, 28.98, 29.21, 29.39, 29.47, 29.70, 29.77, 31.91, 31.97, 32.02, 36.36, 69.91, 105.84, 124.80, 127.81, 138.90, 151.78, 154.98. HRMS-MALDI (*m/z*): [M + H]$^+$ calcd for C$_{108}$H$_{175}$N$_4$O$_4$, 1592.36; found, 1592.35. Anal. Calcd for C$_{108}$H$_{174}$N$_4$O$_4$: C, 81.45; H, 11.01; N, 3.52. Found: C, 81.62; H, 11.10; N, 3.61.

2,11-Bis(1-methylethyl)-6,7,15,16-tetrakis(hexadecyloxy)quinoxaline[2′,3′:9,10]phenanthro[4,5-*abc*]phenazine, TQPP-[*t*-Bu]$_2$-[OC$_{16}$H$_{33}$]$_4$ (1b). Orange solid **1b** (0.62 g, 54%), mp 178−188 °C. ^{1}H NMR (300 MHz, CDCl$_3$): δ 0.86 (12H, t, *J* = 6.7 Hz), 1.26 (96H, m), 1.58 (8H, m), 1.76 (18H, s), 2.02 (8H, quintet, *J* = 7.2 Hz), 4.33 (8H, t, *J* = 6.6 Hz), 7.63 (4H, s), 9.73 (4H, s). ^{13}C NMR (75.5 MHz, CDCl$_3$, 45 °C): δ 14.14, 22.70, 26.13, 28.97, 29.39, 29.46, 29.68, 29.75, 31.95, 35.89, 69.25, 106.99, 122.78, 123.51, 129.58, 139.94, 140.68, 150.26, 153.28. HRMS-MALDI (*m/z*): [M + H]$^+$ calcd for C$_{100}$H$_{159}$N$_4$O$_4$, 1480.23; found, 1480.26. Anal. Calcd for C$_{100}$H$_{158}$N$_4$O$_4$: C, 81.13; H, 10.76; N, 3.78. Found: C, 80.90; H, 10.67; N, 3.81.

2,11-Bis(1-methylethyl)-6,7,15,16-tetrakis(octanethio)quinoxaline[2′,3′:9,10]phenanthro[4,5-*abc*]phenazine, TQPP-[*t*-Bu]$_2$-[SC$_8$H$_{17}$]$_4$ (2c). Yellow solid (1.25 g, 71%), mp > 300 °C. ^{1}H NMR (300 MHz, CDCl$_3$): δ 0.90 (12H, t, *J* = 6.8 Hz), 1.26 (32H, m), 1.61 (8H, pentet, *J* = 7.8 Hz), 1.76 (18H, s), 1.91 (8H, quintet, *J* = 7.4 Hz), 3.25 (8H, t, *J* = 7.3 Hz), 8.10 (4H, s), 9.72 (4H, s). ^{13}C NMR (75.5 MHz, CDCl$_3$): δ 14.14, 22.70, 28.21, 29.23, 31.85, 31.93, 33.36, 35.94, 124.05, 129.32, 140.60, 141.43, 150.68. HRMS-MALDI (*m/z*): [M + H]$^+$ calcd for C$_{68}$H$_{95}$N$_4$S$_4$, 1095.64; found, 1095.65. Anal. Calcd for C$_{68}$H$_{94}$N$_4$S$_4$: C, 74.54; H, 8.65; N, 5.11; S, 11.71. Found: C, 74.37; H, 8.67; N, 5.26; S, 11.42.

2,11-Bis(1-methylethyl)-6,7,15,16-tetrakis(hexanethio)quinoxaline[2′,3′:9,10]phenanthro[4,5-*abc*]phenazine, TQPP-[*t*-Bu]$_2$-[SC$_6$H$_{13}$]$_4$ (2d). Yellow solid (0.61 g, 51%), mp > 300 °C. ^{1}H NMR (300 MHz, CDCl$_3$): δ 0.95 (12H, t, *J* = 7.1 Hz), 1.40 (16H, m), 1.63 (8H, pentet, *J* = 7.2 Hz), 1.77 (18H, s), 1.92 (8H, quintet, *J* = 7.5 Hz), 3.27 (8H, t, *J* = 7.4 Hz), 8.05 (4H, s), 9.70 (4H, s). ^{13}C NMR (75.5 MHz, CDCl$_3$): δ 14.09, 22.59, 28.17, 28.88, 31.45, 31.93, 33.33, 35.92, 123.93, 125.34, 129.37, 140.65, 141.31, 142.15. HRMS-MALDI (*m/z*): [M+H]$^+$ calcd. for C$_{60}$H$_{79}$N$_4$S$_4$, 983.51; found, 983.54. Anal. Calcd. for C$_{60}$H$_{78}$N$_4$S$_4$: C, 73.27; H, 7.99; N, 5.70; S, 13.04. Found: C, 73.04; H, 8.01; N, 5.65; S, 12.73.

2,11-Bis(1-methylethyl)-6,7,15,16-tetrakis(butanethio)quinoxaline[2′,3′:9,10]phenanthro[4,5-*abc*]phenazine, TQPP-[*t*-Bu]$_2$-[SC$_4$H$_9$]$_4$ (2e). Yellow solid (0.87 g, 82%), mp >300 °C. ^{1}H NMR (300 MHz, 1,2-dichlorobenzene-*d*$_4$, 60 °C): δ 0.83 (12H, t, *J* = 7.3 Hz), 1.39 (16H, pentet, *J* = 7.3 Hz), 1.63 (18H, s), 1.68 (8H, quintet, *J* = 7.2 Hz), 3.01 (8H, t, *J* = 7.3 Hz), 8.17 (4H, s), 9.90 (4H, s). HRMS-MALDI (*m/z*): [M + H]$^+$ calcd for C$_{52}$H$_{63}$N$_4$S$_4$, 871.393; found, 871.395. Anal. Calcd for C$_{52}$H$_{62}$N$_4$S$_4$: C, 71.68; H, 7.17; N, 6.43; S, 14.72. Found: C, 71.30; H, 7.05; N, 6.36; S, 14.36.

2.2. Solution Preparation. TQPP-[*t*-Bu]$_2$-[XR]$_4$ (SC4, SC6, SC8, OC16, and OC18) were all dissolved in spectroscopic grade tetrahydrofuran (THF), as this solvent was able to solubilize the entire series efficiently. Several stock solutions were prepared containing 1 mg of these compounds dissolved in sufficient volumes of THF to ensure complete dissolution of each of the compounds; the stock solutions of TQPP-[*t*-Bu]$_2$-[XR]$_4$, therefore, have different concentrations, but in the millimolar concentration range. From these stock solutions, further dilution was made for preparing the 5 μM solutions for absorption spectroscopic measurements. For fluorescence measurements, further dilution to 500 nM was made from the 5 μM stock solution and this concentration was used for further investigation on their photophysical behavior as well as for comparing their behavior with those of previously reported TQPP molecules.[1]

2.3. Spectroscopic Measurement. Absorption spectra were measured using a JASCO V-570 UV−vis-NIR spectrophotom-
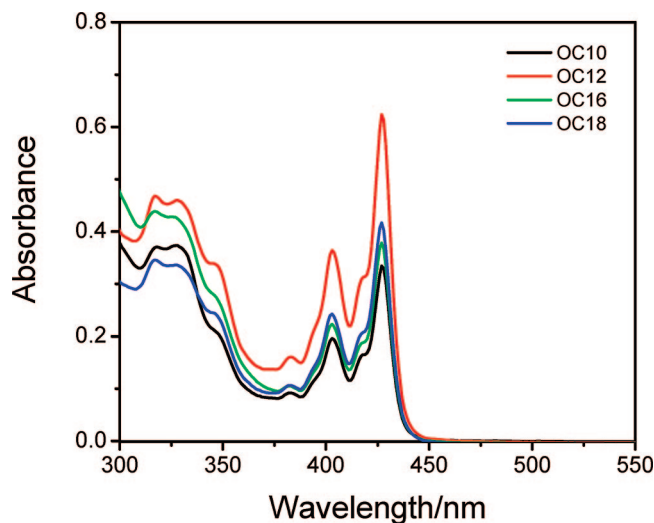
Figure 2. Absorption spectra of TQPP-[*t*-Bu]$_2$-[OR]$_4$ (OC10, OC12, OC16, and OC18) in THF.

Figure 3. Absorption spectra of TQPP-[*t*-Bu]$_2$-[SR]$_4$ (SC4, SC6, SC8, SC10, and SC12) in THF.

Figure 4. Excitation and emission fluorescence spectra of 500 nM TQPP-[*t*-Bu]$_2$-[OR]$_4$ (OC10, OC12, OC16, and OC18) in THF.

eter, and the fluorescence measurements were done using a Jobin-Yvon-Horiba Fluorolog III spectrofluorimeter. The excitation source was a 100 W xenon lamp, and the detector used was R-928 operating at a voltage of 950 V.

2.4. Fluorescence Lifetime Measurement. The fluorescence lifetimes were determined using a Jobin-Yvon-Horiba Fluorolog III spectrofluorimeter with a pulsed diode laser. The decay data were analyzed using Data Analysis software. Decay fits with values of χ^2 between 0.99 and 1.5 were considered to be within the acceptable range.

2.5. Determination of the Fluorescence Quantum Yield. The fluorescence quantum yields of the compounds were determined in THF using the equation:[16]

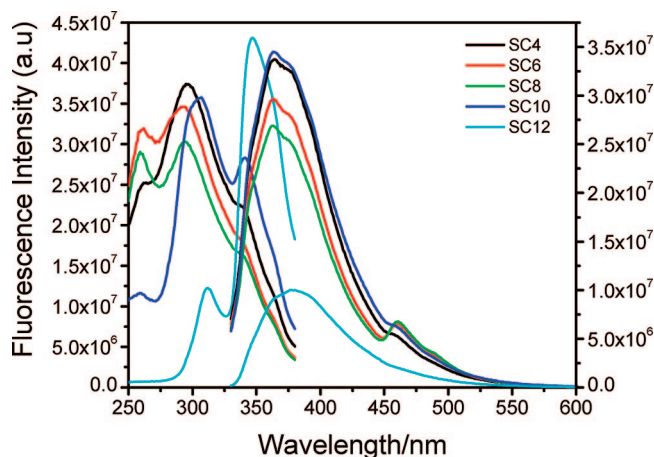$$\phi_{unk} = \phi_{std} \frac{F_{unk}}{F_{std}} \frac{A_{std}}{A_{unk}} \frac{n_{unk}^2}{n_{std}^2} \tag{1}$$

where ϕ_{unk} and ϕ_{std} are the quantum yield of the sample of interest and that of the reference sample, respectively. Anthracene in ethanol was used as the reference, with its quantum yield being taken as 0.31.[17] F_{unk} and F_{std} are the integrated intensities of the emission spectrum of the sample of interest and that of reference sample, respectively. A corresponds to the optical density of the samples at 320 nm, which was used to excite the samples, and finally, n is the refractive index of the solvent being used. In the above equation, standard (std) refers to anthracene in ethanol, and unknown (unk) refers to various TQPP-[*t*-Bu]$_2$-[XR]$_4$ compounds. The fluorescence quantum yields for all compounds were calculated for 500 nM solutions of TQPP-[*t*-Bu]$_2$-[XR]$_4$ in THF.

3. Results and Discussion

The absorption spectra of TQPP-[*t*-Bu]$_2$-[OR]$_4$ and TQPP-[*t*-Bu]$_2$-[SR]$_4$ with various chain lengths are shown in Figures 2 and 3, respectively. Irrespective of the chain length, two absorption features were found in the wavelength regions: one located between 300 and 350 nm, and another between 400 and 475 nm. The absorption bands in the 400−475 nm range showed no shift in absorption maxima and no regular trend in absorbance as the chain length was increased; however, for TQPP-[*t*-Bu]$_2$-[SR]$_4$, the absorption bands around 400−475 nm were 25 nm red-shifted compared to those of TQPP-[*t*-Bu]$_2$-[OR]$_4$, presumably due to the higher polarizability of the sulfur atom compared
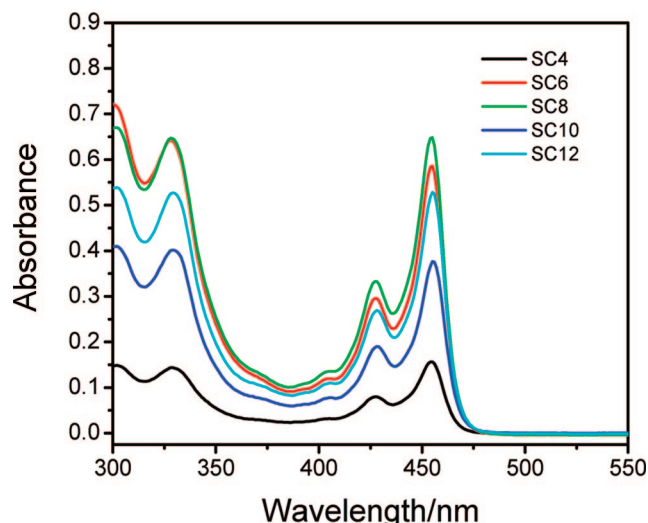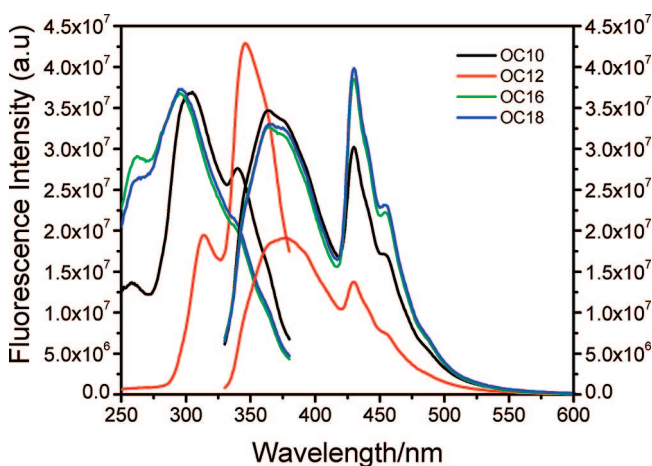
to the oxygen atom. The absorption maximum at around 325 nm showed little change with variation of the carbon chain length from OC10 to OC18 and from SC4 to SC12. However, in both series, slightly longer wavelength absorption maxima were found for the C12 chains (329 nm for TQPP-[*t*-Bu]$_2$-[OC$_{12}$H$_{25}$]$_4$ and 328 nm for TQPP-[*t*-Bu]$_2$-[SC$_{12}$H$_{25}$]$_4$).

The excitation and emission spectra for the TQPP-[*t*-Bu]$_2$-[OR]$_4$ series (OC10, OC12, OC16, and OC18) and the TQPP-[*t*-Bu]$_2$-[SR]$_4$ series (SC4, SC6, SC8, SC10, and SC12) are shown in Figures 4 and 5, respectively. The excitation spectra were collected at an emission wavelength of 390 nm, and the emission spectra were collected at an excitation wavelength of 320 nm. For the TQPP-[*t*-Bu]$_2$-[OR]$_4$ series (Figure 4), two fluorescence emission peaks were observed. Although the fluorescence intensity of these two peaks was different among the series at equimolar concentration, no regular trend was observed. The increase in chain length also did not influence the change in the peak wavelength of the emission maximum. As reported earlier for **1c**, **1d**, **2a**, and **2b** in various solvents,[1] excimer formation was consistently observed for all the TQPP-[*t*-Bu]$_2$-[OR]$_4$ (OC10, OC12, OC16, and OC18). This means, in addition to the monomer peak, a second peak was observed that corresponded to the excimer (excited-state dimer) formation, even at very low concentration (such as 500 nM). The monomer fluorescence peak occurred at around 365−370 nm, whereas

Photophysical Properties of Pyrene-Based Molecules

J. Phys. Chem. A, Vol. 113, No. 7, 2009 **1247**

Figure 5. Excitation and emission fluorescence spectra of 500 nM TQPP-[*t*-Bu]$_2$-[SR]$_4$ (SC4, SC6, SC8, SC10, and SC12) in THF.

TABLE 1: Absorption Maxima, Emission Maxima, and Stokes Shift for TQPP-[*t*-Bu]$_2$-[XR]$_4$ in THF

TQPP-[*t*-Bu]$_2$-[XR]$_4$	λ_{abs} (max)/ nm	λ_{em} (max)/ nm	Stokes shift/ cm^{-1}
SC4	327	364	3109
SC6	327	363	3033
SC8	328	363	2940
SC10	326	381	4428
SC12	328	378	4033
OC10	326	377	4150
OC12	329	376	3799
OC16	326	365	3308
OC18	325	367	3484

the excimer fluorescence peak appeared at around 430 nm. The excimer fluorescence intensity, however, differed for TQPP-[*t*-Bu]$_2$-[OC$_{10}$H$_{21}$]$_4$ and TQPP-[*t*-Bu]$_2$-[OC$_{12}$H$_{25}$]$_4$, but similar excimer intensity was observed for TQPP-[*t*-Bu]$_2$-[OC$_{16}$H$_{33}$]$_4$ and TQPP-[*t*-Bu]$_2$-[OC$_{18}$H$_{37}$]$_4$. Such high excimer intensity for OC16 and OC18 can be explained by the longer chains of these species favoring formation of dimers with $\pi-\pi$ stacking, even at such low concentration (500 nM). However, for OC10 and OC12, such excimer fluorescence intensity was not clearly identifiable, especially for OC12. This can be explained by the assumption that, for TQPP-[*t*-Bu]$_2$-[OC$_{12}$H$_{25}$]$_4$, the best geometry for such compounds was not a two-dimensional structure, but rather the long chain groups were arranged in such a way that impeded proper $\pi-\pi$ stacking and thus lowered the possibility of excimer formation.

Also for the TQPP-[*t*-Bu]$_2$-[SR]$_4$ series (Figure 5), similar behavior concerning excimer formation was observed. A monomer fluorescence peak was observed for all the SC4, SC6, SC8, SC10, and SC12 series at around 370 nm, and an excimer peak at around 462 nm. For SC4, SC6, and SC8, a gradual small increase in the intensity of the excimer peak was observed. This is consistent with increased $\pi-\pi$ overlap and excimer formation, as the chain length is increased from SC4 to SC8. However, for SC10 and SC12, a different behavior was observed. For SC10, because of higher chain length, a higher excimer peak intensity than that of SC8 was expected, but it was found to be lower, and for SC12 no excimer peak was observed at similar concentrations. SC10 and SC12 may also exhibit the same behavior as that of OC10 and OC12, in that perhaps such compounds are not entirely two-dimensional, preventing excimer formation at such low concentration. Nevertheless, sulfur is more polarizable than oxygen, which may also play a role in preventing proper arrangements of the compounds and the formation of excimers. The fluorescence spectra of TQPP-[*t*-Bu]$_2$-[SR]$_4$ displayed clear excimer peaks for each of the SC4, SC6, and SC8 derivatives, but not for SC10 and SC12 even at equimolar concentration (500 nM). The assumption that chain length is a factor in enhancing the rate of excimer formation leads to the conclusion that SC10 and SC12 should show excimer peaks. However, this was not the case. The reason may be that SC10 and SC12 compounds are prevented from adopting a two-dimensional conformation and, therefore, from π-stacking to form excimers, due to an orientation of the four alkyl chains. Comparing the sulfur-containing (SC10 and SC12) and oxygen-containing (OC10 and OC12) pyrene-based molecules that have the same number of carbons at the same concentration, we

observed the formation of clear excimer peak for the O-series and yet the absence or the negligible appearance of the excimer peak for the S-series.

The absorption maxima, emission maxima, and Stokes shift for TQPP-[*t*-Bu]$_2$-[SR]$_4$ and TQPP-[*t*-Bu]$_2$-[OR]$_4$ molecules in THF are reported in Table 1. The emission wavelength maximum for all the compounds in the two series was almost unaltered. No regular trend was observed for the Stokes shift as the chain length increased from C4 to C12 in the case of TQPP-[*t*-Bu]$_2$-[SR]$_4$ or from C10 to C16 in the case of TQPP-[*t*-Bu]$_2$-[OR]$_4$ (Figure 6). However, when the Stokes shift of the different C10 and C12 TQPP molecules were compared, higher values for those of the sulfur-based TQPP molecules compared to the oxygen-based ones were observed, perhaps again due to the higher polarizability of the sulfur atom compared to that of oxygen.

The monomer and excimer fluorescence lifetimes, fluorescence quantum yield, and radiative and nonradiative rate constants are reported for the TQPP-[*t*-Bu]$_2$-[SR]$_4$ and TQPP-[*t*-Bu]$_2$-[OR]$_4$ series in Table 2. The lifetime decays for the oxygen-based series and those of the sulfur-based series are also, respectively, shown in Figures 7 and 8; all compounds showed a biexponential lifetime decay, with one of these decays being attributed to that of the monomer and the other to the excimer.[18] The monomer lifetimes range between 3 and 5 ns, whereas the excimer lifetimes range between 11 and 13 ns. For TQPP-[*t*-Bu]$_2$-[SR]$_4$, the monomer lifetime decreased in going from SC4 to SC8 with a significant increase for SC10, followed by a further decrease for SC12. The trend was similar for TQPP-[*t*-Bu]$_2$-[OR]$_4$ in going from OC10 to OC18. When monomer
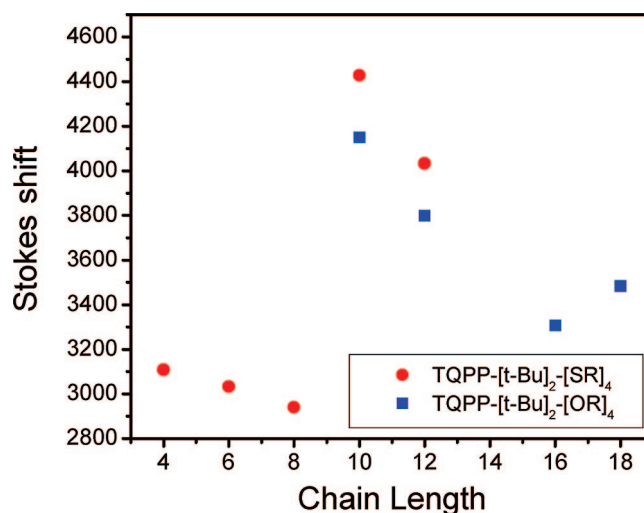
Figure 6. Stokes shift in THF versus chain length of TQPP-[*t*-Bu]$_2$-[XR]$_4$.

TABLE 2: Monomer Lifetime, Excimer Lifetime, Fluorescence Quantum Yield, and Radiative and Nonradiative Rate Constants of TQPP-[*t*-Bu]₂-[XR]₄ at 25 °C in THF

TQPP-[*t*-Bu]₂-[XR]₄	$\tau_{monomer}$/ ns	$\tau_{excimer}$/ n	ϕ_f	k_r/ $(10^8\ s^{-1})$	k_{nr}/ $(10^8\ s^{-1})$
SC4	3.32	12.03	0.22	0.64	2.37
SC6	3.14	11.78	0.23	0.73	2.45
SC8	3.06	11.75	0.20	0.64	2.63
SC10	4.85	11.95	0.09	0.19	1.88
SC12	3.99	12.34	0.15	0.37	2.14
OC10	4.17	12.83	0.02	0.05	2.35
OC12	3.65	11.27	0.09	0.25	2.49
OC16	3.69	12.04	0.26	0.70	2.01
OC18	3.18	11.74	0.27	0.86	2.28

lifetimes for SC10 and SC12 with those of OC10 and OC12 were compared, higher monomer lifetimes were observed in the sulfur-based TQPP molecules. The excimer lifetime, how-

Figure 7. Lifetime decays for TQPP-[*t*-Bu]₂-[SR]₄ (SC4, SC6, SC8, SC10, and SC12) in THF. Theoretical fittings are not shown for clarity; in all cases, the best results were obtained for a bioexponential decay (one representing monomer, and the other excimer) with an acceptable χ^2 value between 0.99 and 1.5.

Figure 8. Lifetime decays for TQPP-[*t*-Bu]₂-[OR]₄ (OC10, OC12, OC16, and OC18) in THF. Theoretical fittings are not shown for clarity; in all cases, the best results were obtained for a bioexponential decay (one representing monomer, and the other excimer) with an acceptable χ^2 value between 0.99 and 1.5.

ever, did not show any regular trend among the different compounds. The fluorescence quantum yields were calculated to be around 0.2 for most of the TQPP-[*t*-Bu]₂-[XR]₄ molecules in THF. However, for the SC10, OC10, and OC12 derivatives, the fluorescence quantum yields were found to be considerably smaller (0.09, 0.02, and 0.09, respectively). The radiative (k_r) and nonradiative (k_{nr}) rate constants were calculated, for all TQPP-[*t*-Bu]₂-[XR]₄ in THF, using the following two equations, respectively:[19]

$$k_r = \frac{\phi_f}{\tau_f}$$

$$k_{nr} = \frac{1}{\tau_f} - k_r$$

where ϕ_f is the fluorescence quantum yield and τ_f is the fluorescence lifetime.

The radiative rate constants for all TQPP-[*t*-Bu]₂-[XR]₄ molecules were of the order of $10^7\ s^{-1}$, and the nonradiative rate constants were of the order of $10^8\ s^{-1}$. In all cases, the radiative and nonradiative rate constants were notably larger than those for pyrene itself, which are of the order of $10^6\ s^{-1}$. The radiative and nonradiative rate constants for the SC10 compound were lower than those of the SC12 example. In addition, rate constants for the OC10 derivative were lower than those for the OC12 species. However, no regular trend was found for the radiative and nonradiative rate constants as the chain length increased. Furthermore, no correlation could be found between the radiative or nonradiative rate constants and the change in the chain length of substituents.
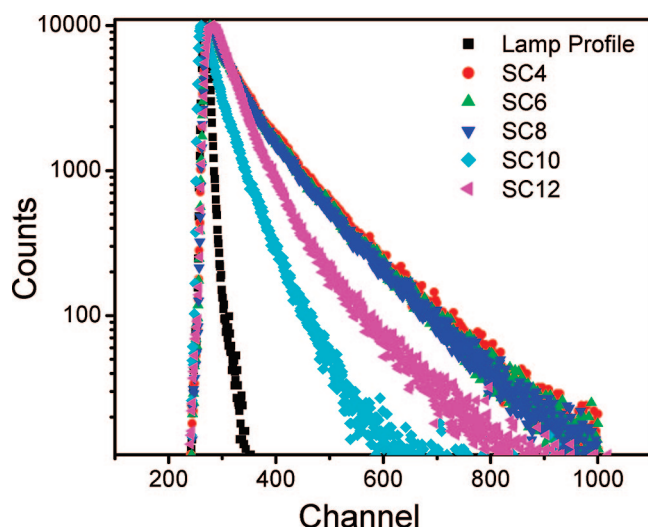
4. Conclusion

As an extension of our previous work, more TQPP-[*t*-Bu]₂-[XR]₄ (X = O, S) compounds have been introduced in this paper. The photophysical properties of these novel compounds were revealed in correlation with the change in the number of carbons of the four alkyl chains. Stokes shift, fluorescence quantum yield, fluorescence lifetime, and radiative and nonradiative rate constants are all reported for both oxygen-based and sulfur-based series. No linear correlation was observed for the Stokes shift, fluorescence quantum yield, and radiative or nonradiative rate constants as a function of the chain length of the four alkyl chains of these pyrene-based molecules.
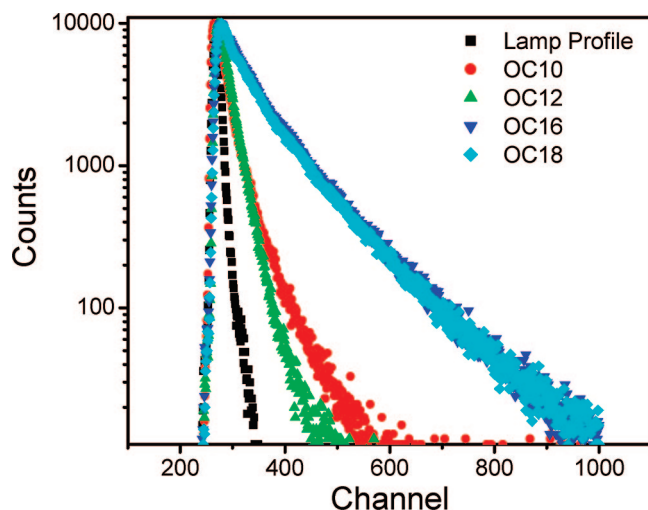
References and Notes

(1) Moustafa, R. M.; Degheili, J. A.; Patra, D.; Kaafarani, B. R. *J. Phys. Chem. A.* Submitted for publication.

(2) Mitzi, D. B. *J. Mater. Chem.* **2004**, *14*, 2355.

(3) Ponomarenko, S. A.; Kirchmeyer, S.; Elschner, A.; Huisman, B.-H.; Karbach, A.; Drechsler, D. *Adv. Funct. Mater.* **2003**, *13*, 591.

(4) Naraso; Nishida, J.; Ando, S.; Yamaguchi, J.; Itaka, K.; Koinuma, H.; Tada, H.; Tokito, S.; Yamashita, Y. *J. Am. Chem. Soc.* **2005**, *127*, 10142.

(5) Palilis, L. C.; Murata, H.; Uchida, M.; Kafafi, Z. H. *Org. Electron.* **2003**, *4*, 113.

Photophysical Properties of Pyrene-Based Molecules

J. Phys. Chem. A, Vol. 113, No. 7, 2009 **1249**

(6) Oukachmih, M.; Destruel, P.; Seguy, I.; Ablart, G.; Jolinat, P.; Archambeau, S.; Mabiala, M.; Fouet, S.; Bock, H. *Sol. Energy Mater. Sol. Cells* **2005**, *85*, 535.

(7) Anthony, J. E. *Angew. Chem., Int. Ed.* **2008**, *47*, 452.

(8) Chen, M.-C.; Kim, C.; Chen, S.-Y.; Chiang, Y.-J.; Chung, M.-C.; Facchetti, A.; Marks, T. J. *J. Mater. Chem.* **2008**, *18*, 1029.

(9) Sun, Y.; Rogers, J. A. *Adv. Mater.* **2007**, *19*, 1897.

(10) Kumar, S. *Chem. Soc. Rev.* **2006**, *35*, 83.

(11) Chen, Z.; Mueller, P.; Swager, T. M. *Org. Lett.* **2006**, *8*, 273.

(12) Petritsch, K.; Friend, R. H.; Lux, A.; Rozenberg, G.; Moratti, S. C.; Holmes, A. B. *Synth. Met.* **1999**, *102*, 1776.

(13) Katsuhara, M.; Aoyagi, I.; Nakajima, H.; Mori, T.; Kambayashi, T.; Ofuji, M.; Takanishi, Y.; Ishikawa, K.; Takezoe, H.; Hosono, H. *Synth. Met.* **2005**, *149*, 219.

(14) Boden, N.; Bushby, R. J.; Clements, J.; Movaghar, B. *J. Mater. Chem.* **1999**, *9*, 2081.

(15) Van de Craats, A. M.; Warman, J. M.; Fechtenkötter, A.; Brand, J. D.; Harbison, M. A.; Müllen, K. *Adv. Mater.* **1999**, *11*, 1469.

(16) Parker, C. A. *Photoluminescence of Solutions with Applications to Photochemistry and Analytical Chemistry*; Elsevier, Amsterdam, 1968.

(17) Subuddhi, U.; Haldar, S.; Sankararaman, S.; Mishra, A. K. *Photochem. Photobiol. Sci.* **2006**, *5*, 459.

(18) Waris, R.; Rembert, M. A.; Sellers, D. M.; Acree, W. E., Jr.; Street, K. W., Jr.; Poole, C. F.; Shetty, P. H.; Fetzer, J. C. *Appl. Spectrosc.* **1988**, *42*, 1525.

(19) Lakowicz, J. R. *Principles of Fluorescence Spectroscopy*; Kluwer Academic, Plenum Publishers: NewYork, 1999.